Eurographics Workshop on Visual Computing for Biology and Medicine (2018)
I. Hotz, B. Kozlikova, and P.-P. Vazquez (Editors)

A New Vessel Enhancement Transform on Retinal Blood Vessels Segmentation

Ivo Soares[1,2] and Miguel Castelo-Branco[1] and António M. G. Pinheiro[2]

[1]Health Sciences Research Centre, University of Beira Interior (CICS-UBI), Av. Infante D. Henrique, 6200-506, Covilhã, Portugal
[2]Instituto de Telecomunicações, Universidade da Beira Interior, R. Marques D'Avila e Bolama, 6200-001 Covilhã, Portugal

Abstract

The automatic detection of retinal blood vessels is a very important task in computer aided-diagnosis of retinal diseases. In this work a new method is proposed for the automated detection of the retinal vessels. Three new and important contributions are made. First, a new method capable of vessel enhancement is presented. Second, a new criterium to remove some false vessels caused by the proximity to bright regions is presented, avoiding the false vessels created by the presence of exudates or bright artifacts. Third, a new method that discards the false vessel regions that usually tends to appear in the border of the optic disc. This is achieved using the derivatives of the gradient magnitude local maxima over different scales. The performance evaluation is made on two publicly available databases, namely, STARE, and HRF with state-of-the-art results. Particularly, the described method reveals to be very reliable on retinal images with large pathological signs.

CCS Concepts

• ***Computing methodologies*** → ***Image segmentation;*** • ***Applied computing*** → *Imaging;*

1. Introduction

Several systemic and non-systemic diseases are exposed through changes in the retinal blood vessels [XNS*11]. Furthermore, the eye is unique since its the only region of the human body where the vascular network can be observed in vivo [MC06]. The analysis of the retinal vasculature is fundamental in glaucoma, diabetic retinopathy, hypertensive retinopathy, cardiovascular diseases, and other cerebral diseases like stroke [XNS*11, PPP16]. In the case of diabetic retinopathy, which is the second most common cause of blindness in the developed world, vascular changes include neovascularization, and hemorrhages. Hypertension and atherosclerosis also cause changes in the ratio between the diameter of retinal arteries and veins. Thinning of the arteries and widening of the veins is associated with an increased risk of a stroke and myocardial infarction [XNS*11]. The manual segmentation of the retina vessels is a very time consuming task and prone to errors [AGB*16]. Hence, the automatic quantification of the retinal vessels as well the vascular features, such as the length, width, tortuosity, branching pattern, and arteries/veins differentiation can provide important insights to a proper diagnose and management of the previous mentioned diseases. The accurate segmentation of the retinal vessels is a challenging task for several reasons: the presence of lesions, exudates, and hemorrhages; other structures like the optic disc and fovea; a wide range of scales; variable contrast between the vessels and retina background, and the central reflex in major arteries [AGB*16].

Many methods have been reported for the segmentation of the retinal vessels. These can be divided into two major groups: Supervised methods and rule-based methods [PPP16, AGB*16]. The proposed method is rule-based. Supervised methods require manually labeled images data used as training sets for each image pixel classification. The rule-based methods do not use any prior labelling knowledge. The most common used techniques include matching filtering, morphological processing, vessel tracking, multi-scale analysis, and model based algorithms [AGB*16]. A detailed review of recent blood vessel segmentation methods can be found in [MMHM18, LSAR17]. In this paper a reliable and efficient method for the automated detection of the retinal blood vessels in retinal images is presented. Several new and important contributions are made. Firstly, a method capable of vessel enhancement based on the differences between the neighborhood of intensities of a given pixel and the pixel itself is developed. Based on this enhancement method it is possible to perform the detection and segmentation of the retinal vessels over a large range of widths, lengths and orientations. Secondly, a set of new criteria that remove false vessels branches caused by the presence of bright features like the optic disc and yellowish lesions. Finally, a new approach to remove regions of peripapillary atrophy that appear near the borders of the optic disc that are misidentified as vessels, is also established. The performance evaluation is made using two public databases, namely, STARE [STA] and HRF [OKB*13]. The rest of the paper is organized as follows. Section 2 describes the proposed method and its three main stages; 1) Image pre-processing, 2) Vessel enhancement and 3) Vessel segmentation. Experimental results

DOI: 10.2312/vcbm.20181237

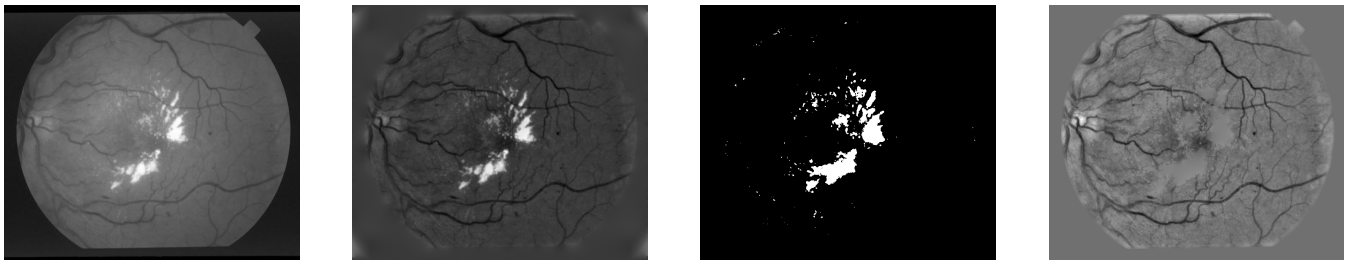

(a) $I_G(\boldsymbol{x})$ **(b)** $I_P(\boldsymbol{x})$ **(c)** $B_L(\boldsymbol{x})$ **(d)** $I_F(\boldsymbol{x})$

Figure 1: *Image pre-processing steps.*

are described and discussed in Section 3. Finally, some concluding remarks are drawn in Section 4.

2. Proposed Method

The proposed method is divided into three stages; 1) Image pre-processing, 2) Retinal vessels enhancement and 3) Retinal vessels segmentation.

2.1. Image pre-processing

The image pre-processing stage normalizes the images in terms of contrast and non-uniform illumination. The scale-space and differential operators used in this work are also defined. The green channel component $I_G(\mathbf{x})$ (where $\mathbf{x}$ represents the location (x,y)) of each *RGB* retinal image is selected, since it offers the best contrast between image features [WMM09] (see Figure 1 a)). If not provided, the Black-and-White masks $BW(x)$, that define the region of interest in $I_G(\mathbf{x})$, are created by selecting all the pixels in the red channel of the *RGB* image larger than 35 [tH05]. Next, if the image dimensions are large, $I_G(\mathbf{x})$ is proportionally resized using a bicubic interpolation, such that its smaller dimension is 700 pixels. The size normalization allows the definition of a set of algorithm parameters that are effective in all databases. To remove background lightening variations, a shade-correction algorithm is performed [AGB*16, MAGAB11]. First, an inpainting algorithm performs a smooth interpolation of the peripheral pixels of $I_G(\mathbf{x})$. This is done with a discretization of the Laplace's equation $\nabla^2 I(\mathbf{x}) = 0$ [LOD12], creating the image $I_P(\mathbf{x})$ (see Figure 1 b)). Next, a median filtering with a mask size $[89 \times 89]$ is applied to $I_P(\mathbf{x})$. This large filter is necessary to create an image representation of the lightning variation in $I_P(\mathbf{x})$ and is designated by $I_M(\mathbf{x})$. The shade-correction algorithm ends by subtracting $I_M(\mathbf{x})$ from $I_P(\mathbf{x})$, creating the image $I_S(\mathbf{x}) = I_P(\mathbf{x}) - I_M(\mathbf{x})$. The next step is the detection and removal of bright regions in $I_S(\mathbf{x})$. These bright regions may represent exudative lesions, central arterial reflex or belong to the optic disc. In any case they can complicate vessel segmentation. Initially the bright regions image, $B_L(\mathbf{x})$ is created by thresholding $I_S(\mathbf{x})$ and selecting all pixels larger than 12. Next, the optic disc is detected using the method proposed in [SCBP16]. A binary image $OD(\mathbf{x})$ where the pixel of the optic disc center has a value of 1 and all the remaining pixels have a value of 0 results. This point is then dilated by a 'disk' structuring element of size 60. This value is sufficient to cover both smaller and larger discs. All the regions in $B_L(\mathbf{x})$ that intersect slightly or full the optic disc region in $OD(\mathbf{x})$ are removed.

Finally, the peripheral regions in $B_L(\mathbf{x})$ are also removed. This is achieved by considering an inverted eroded $BW(\mathbf{x})$ image with a structuring disk element of size 20. All the regions in $B_L(\mathbf{x})$ that intersect in part or full this inverted image are removed (see Figure 1 c)). The image pre-processing stage is finalized with the inpainting of $I_S(\mathbf{x})$ in the $B_L(\mathbf{x})$ regions, using the previously described inpainting method. This creates the final processed image $I_F(\mathbf{x})$ (see Figure 1 d)).

2.1.1. Differential operators definition in scale-space

Retinal blood vessels have a wide range of scales, which makes a scale-space analysis ideal for their detection. The used scale-space was defined in [SCBP14] and is briefly described next. A family of derived images is defined by the convolution of $I_F(\mathbf{x})$ with the Gaussian filter $g(\mathbf{x};t)$, are given by,

$$L(\mathbf{x};t) = g(\mathbf{x};t) * I_F(\mathbf{x}), \forall t. \tag{1}$$

where $g(\mathbf{x};t) = \frac{1}{\sqrt{2\pi t}} e^{-\frac{|\mathbf{x}|^2}{2t}}$ is the Gaussian kernel and $*$ represents the convolution [Wit83]. $2t$ is the variance of the Gaussian filter, where t represents the scale. t is defined in this work at N different scales according to $t_n = n\frac{\sqrt{2}}{4}$, with $n \in \{1,...,N\}$ ($n = 0$ represents the initial pre-processes image $I_F(\mathbf{x})$). N was set to 20. Due to the noise present in the lower scale, t_0 was discarded. The first and second order image derivatives $L_x(\mathbf{x};t_n)$ and $L_{xx}(\mathbf{x};t_n)$ are calculated with the derivative mask $[-1\ 0\ 1]$. The derivative mask transpose is used to compute the derivatives in the y direction, namely $L_y(\mathbf{x};t_n)$ and $L_{yy}(\mathbf{x};t_n)$. To obtain a normalized response at each scale t_n, the derivatives are multiplied by the normalization factor $(t_n\sigma)^\alpha$ where α is the order of the derivative [MPHT*07]. Considering the image $L(\mathbf{x};t_n)$ as an intensity surface, it is possible to describe the local shape characteristics $(\mathbf{x};t_n)$ using the Hessian matrix,

$$H(\mathbf{x};t_n) = \begin{bmatrix} L_{xx}(\mathbf{x};t_n) & L_{xy}(\mathbf{x};t_n) \\ L_{yx}(\mathbf{x};t_n) & L_{yy}(\mathbf{x};t_n) \end{bmatrix}. \tag{2}$$

The minimum and maximum principal curvatures of $H(\mathbf{x};t_n)$ at $(\mathbf{x};t_n)$ are represented by $\lambda_1(\mathbf{x};t_n)$ and $\lambda_2(\mathbf{x};t_n)$ respectively [DZM*07].

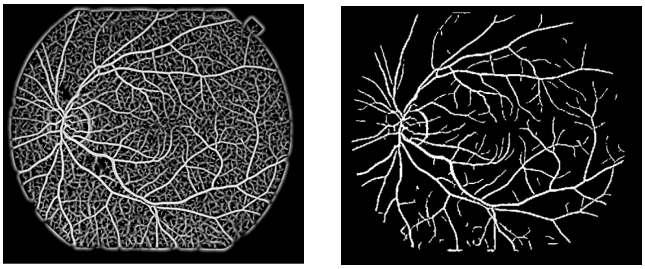

(a) $E(\boldsymbol{x})$ **(b)** $V(\boldsymbol{x})$

Figure 2: *Retinal vessel enhancement.*

2.2. Retinal vessel enhancement

In this section a new retinal vessel enhancement transform is defined. The maximum principal curvature $\lambda_2(\mathbf{x};t_n)$ is commonly used for vessels structures enhancement [MLG*18]. To improve the enhancement, a cumulative maximum over scales of the principal curvature $\lambda_2(\mathbf{x};t_n)$ is proposed. Considering a scale t_u where $u \in \{1,...,N\}$. For all scales t_u, such that $u \leq n$, the proposed cumulative maximum over scales of the principal curvature $\lambda_2(\mathbf{x};t_n)$ is given by,

$$\Lambda_u(\mathbf{x}) = \max_{u \leq n} \left(\frac{\lambda_2(\mathbf{x};t_u)}{(t_u \sigma)^2} \right), \tag{3}$$

Retinal vessels have a large variation of intensity values in a given direction, while in the perpendicular direction the intensity values variation is small. If a difference is made between $\Lambda_u(\mathbf{x})$ and $\Lambda_u(\mathbf{x'})$, where **x'** is a pixel location in a neighborhood of **x**, a response is obtained. To further improve the vessels enhancement, it is necessary to consider all neighborhood pixels of **x**. The neighborhood itself has to be widened due to the various widths that vessels can have. Furthermore, if performed in scale-space the effects of noise is reduced. Formally, this can be expressed using a polar framework. For every pixel location **x** a neighborhood pixel at a range ρ and angle θ given by $\mathbf{x}_{(d,\theta)}$ is defined. The final retinal vessel enhancement operator is given by,

$$E(\mathbf{x}) = \sum_{t_u} \left(\sum_{\theta} \sum_{\rho} \left(\Lambda_u(\mathbf{x}_{(\rho,\theta)}) - \Lambda_u(\mathbf{x}) \right) \right). \tag{4}$$

The parameters ρ and θ vary according to the set of values $\rho = \{1,2,...,5\}$ and $\theta = \{22.5^o, 45^o, ..., 360^o\}$ (see Figure 2 a)).

2.3. Retinal vessels segmentation

In this section the segmentation of retinal vessels is described. Firstly, $E(\mathbf{x})$ is thresholded with two different values, T_1 and T_2, defining a hysteresis selection where only a percentage of its maxima are selected. The threshold value T_1 creates the binary image $V_{T_1}(\mathbf{x})$ and its regions are considered vessel seeds. The value T_2 creates the binary image $V_{T_2}(\mathbf{x})$ and its regions represent a more complete definition of the vessels branches in terms of shape, length and width. Regions in $V_{T_1}(\mathbf{x})$ smaller than 30 pixels are removed to avoid overseeding and a final oversegmentation. Furthermore, vessel seeds that are too close to bright regions in $B_L(\mathbf{x})$ are most likely artifacts and are removed. For any vessel seed region, the mean distance of its perimeter pixels to the bright regions in $B_L(\mathbf{x})$ is determined. If it is closer than eight pixels, the vessel seed is removed from $V_{T_1}(\mathbf{x})$.

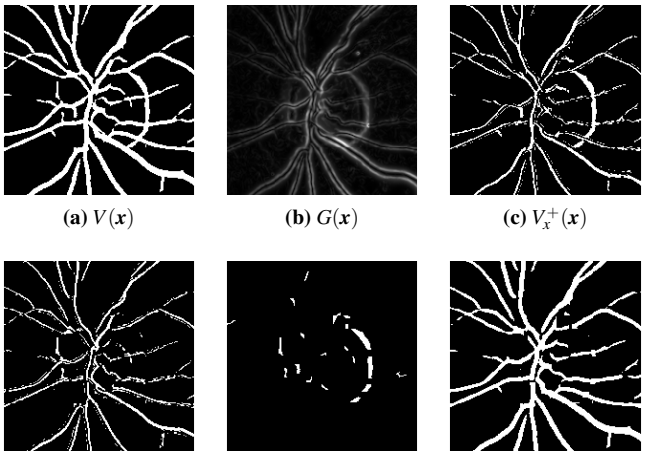

(a) $V(\boldsymbol{x})$ **(b)** $G(\boldsymbol{x})$ **(c)** $V_x^+(\boldsymbol{x})$

(d) $V_x^-(\boldsymbol{x})$ **(e)** $R(\boldsymbol{x})$ **(f)** $V_F(\boldsymbol{x})$

Figure 3: *Peripapillary atrophy regions removal.*

The next step is a normalization between 0 and 1 of $\Lambda_u(\mathbf{x})$ for all the scales, that is, when $u = n$, followed by a histogram equalization (64 levels). A binarization is then performed using a threshold of 0.85, resulting in $\Lambda_B(\mathbf{x})$ [SCBP14]. An initial vessel segmentation $V(\mathbf{x})$ is obtained by selecting all the regions in $V_{T_1}(\mathbf{x})$ that intersect the regions in $V_{T_2}(\mathbf{x})$ and also the regions in $\Lambda_B(\mathbf{x})$ as represented in Figure 2) b). Usually, along the optic disc borders appear darker regions of peripapillary atrophy. Due to its low pixel values they are misidentified as a vessel (see Figure 3 a)). Even if the optic disc was previously removed before the retinal vessel enhancement, these regions will still be present because of the required feature preservation. These false regions are removed based on the normalized maximum over different scales of the gradient magnitude, given by,

$$G(\mathbf{x}) = \max_{t_n} \left(\frac{|\nabla L(\mathbf{x};t_n)|}{(t_n \sigma)} \right), \tag{5}$$

and the sign of its derivatives $G_x(\mathbf{x})$ and $G_y(\mathbf{x})$. The process is first explained to the x-direction. $G_x(\mathbf{x})$ is calculated by the convolution of $G(\mathbf{x})$ with the mask $[-1\ 0\ 1]$. The vessels in $V(\mathbf{x})$ have a gaussian profile. This means that if a vessel is divided along its centerline, $G_x(\mathbf{x})$ has positive or negative values on each side of the centerline [MC06]. Darker regions near the optic disc border do not exhibit a gaussian profile, meaning that its regions have either negative or positive values in $G_x(\mathbf{x})$. These regions in $V(\mathbf{x})$ are detected by the $sgn(G_x(\mathbf{x}))$, where $sgn(.)$ stands for the sign function, according to,

$$\begin{aligned} V_x^+(\mathbf{x}) &= V(\mathbf{x}) sgn(G_x(\mathbf{x})) : G_x(\mathbf{x}) > 0, \\ V_x^-(\mathbf{x}) &= V(\mathbf{x}) sgn(G_x(\mathbf{x})) : G_x(\mathbf{x}) < 0. \end{aligned} \tag{6}$$

$V_x^+(\mathbf{x})$ and $V_x^-(\mathbf{x})$ represents the positive and negative values of the darker regions near the optic disc border (see Figure 3 c) and

d)). When $V_x^+(\mathbf{x})$ and $V_x^-(\mathbf{x})$ are compared to $V(\mathbf{x})$, only half the vessels are present, but darker regions near the optic disc border either suffers no change or totally disappear. A line scan search is performed in $V(\mathbf{x})$ to determine the regions that either suffer no change or completely disappears in $V_x^+(\mathbf{x})$ and $V_x^-(\mathbf{x})$. These regions are saved in $R_x(\mathbf{x})$. The above process is repeated along the y-direction creating the image $R_y(\mathbf{x})$. The darker regions near the optic disc border are given by $R(\mathbf{x}) = R_x(\mathbf{x}) + R_y(\mathbf{x})$. Spurious regions in $R(\mathbf{x})$ smaller than 10 pixels are discarded. Furthermore, the regions in $R(\mathbf{x})$ that do not intersect the regions in $OD(x)$ are discarded (see Figure 3 e)). The final segmented vessels $V_F(\mathbf{x})$, represented in Figure 3 f) are given by,

$$V_F(\mathbf{x}) = V(\mathbf{x}) - R(\mathbf{x}). \tag{7}$$

3. Results and discussion

In this paper a new method for the automated detection of the retinal vessels is presented. To evaluate the proposed algorithm two publicly available databases were used, namely the STARE and the HRF. The STARE database [HG03] is composed by 10 images of healthy retinas and 10 images of pathological retinas. The images were captured by a TopCon TRV-50 fundus camera at 35^o of field view. Each slide was digitized to produce a 605x700 pixel image, with 24 bit per pixel. Each of the 20 images were hand labeled by two manual experts, namely, AH and VK. As it is common in previous works using this database, the AH segmented images are used as the groundtruth [MPHT*07]. The High-Resolution Fundus (HRF) Image database [OKB*13] is composed by 45 images, divided into three sets of 15 images each with healthy retinas, retinas affected with glaucoma, and retinas affected with diabetic retinopathy. The images were acquired with a CANON CF-60 UVi equipped with a CANON EOS-20D digital fundus camera with 60^o FOV. Each image has its retinal vessels segmentation groundtruth. To evaluate the performance, the vessel segmentation resulting in $V_F(\mathbf{x})$ is compared to its groundtruth. If a vessel pixel in $V_F(\mathbf{x})$ belongs to a blood vessel in the groundtruth is a true positive (TP), otherwise if it belongs to the background is a false positive (FP). If a background pixel in $V_F(\mathbf{x})$ belongs to the background in the groundtruth image it is a true negative (TN), otherwise if it belongs to a blood vessel in the groundtruth is a false negative (FN). The evaluation of the propose method is performed in terms of Sensitivity (SE), Specificity (SP) and Accuracy (ACC). SE is the ratio of correctly classified pixels and SP is the ratio of corrected classified non vessel pixels. ACC is the proportion of true results considering the total number of pixels. These metrics are defined as, $SE = \frac{TP}{TP+FN}$, $SP = \frac{TN}{TN+FP}$, and $ACC = \frac{TP+TN}{TP+TN+FP+FN}$. The average sensitivity, specificity and accuracy accomplished by the proposed method is 0.7126, 0.9758 and 0.9482 for the STARE database. For the HRF database the average sensitivity, specificity and accuracy are, 0.7384, 0.9727 and 0.9521 respectively. A comparison with the existing methodologies is presented in Table 1. Figure 4 shows some segmentation results of a image, of each testing database. From Table 1 it is possible to observe that the proposed method achieves comparable results with existing methodologies. This is particularly relevant considering that both databases represent images with pathological signs, making the accurate detection and segmentation of retinal vessels a bigger challenge. Furthermore, the proposed algorithm is a deterministic method that requires no training, with the ability to overcome the presence of bright lesions like exudates or drusens. All thresholds of the proposed algorithm were defined after extensive testing. In particular the T_1 and T_2 percentage values were defined as $T_1 = 7\%$ and $T_2 = 20\%$.

	STARE			HRF		
Method	SE	SP	ACC	SE	SP	ACC
Panda *et al.* [PPP16]	—	—	—	0.8159	0.9508	0.8407
Christodoulidis *et al.* [CHTC16]	—	—	—	0.8506	0.9582	0.9479
Orlando *et al.* [OPB17]	0.8951	0.9387	—	0.7874	0.9584	—
Kovacs *et al.* [KH16]	0.8034	0.9786	0.9610	0.7502	0.9868	0.9674
Zhang *et al.* [ZDB*16]	0.7791	0.9758	0.9554	0.7978	0.9717	0.9556
Yu *et al.* [YBA*12]	0.7112	—	0.9463	0.7938	—	0.9566
Budai *et al.* [OKB*13]	0.5800	0.9820	.09386	0.6690	0.9850	0.9610
Annunziata *et al.* [AGB*16]	0.7128	0.9836	0.9562	0.7128	0.9836	0.9581
Azzopardi *et al.* [ASVP15]	0.7716	0.9701	0.9497	—	—	—
Our Method	0.7126	0.9758	0.9482	0.7384	0.9727	0.9521

Table 1: *Segmentation results of the proposed method and some well known methods.*

4. Conclusion and future works

In this paper, an effective methodology for the automatic segmentation of the retinal vessels is presented with several important contributions: 1) a new retinal vessel enhancement method and 2) a new approach to remove darker regions near the optic disc borders based on differential operators. The method depends on several fixed values. Improvements are currently being implemented in terms of dynamic thresholding to improve there stabilization. Furthermore, the final segmentation result exhibits some disconnected vessels as well small vessels that are not detected. The implementation of new pre-processing methods and supervised techniques are currently being developed to overcome this situation.

References

[AGB*16] ANNUNZIATA R., GARZELLI A., BALLERINI L., MECOCCI A., TRUCCO E.: Leveraging multiscale hessian-based enhancement with a novel exudate inpainting technique for retinal vessel segmentation. *IEEE J. Biomed. Health. Inf. 20*, 4 (July 2016), 1129–1138. 1, 2, 4

[ASVP15] AZZOPARDI G., STRISCIUGLIO N., VENTO M., PETKOV N.: Trainable cosfire filters for vessel delineation with application to retinal images. *Med. Image Anal. 19*, 1 (2015), 46 – 57. 4

[CHTC16] CHRISTODOULIDIS A., HURTUT T., TAHAR H. B., CHERIET F.: A multi-scale tensor voting approach for small retinal vessel segmentation in high resolution fundus images. *Comput Med Imaging Graph 52* (2016), 28 – 43. 4

[DZM*07] DENG H., ZHANG W., MORTENSEN E., DIETTERICH T., SHAPIRO L.: Principal curvature-based region detector for object recognition. In *Computer Vision and Pattern Recognition, 2007. CVPR '07. IEEE Conference on* (June 2007), pp. 1–8. 2

[HG03] HOOVER A., GOLDBAUM M.: Locating the optic nerve in a retinal image using the fuzzy convergence of the blood vessels. *IEEE Trans. Med. 22*, 8 (2003), 951–958. 4

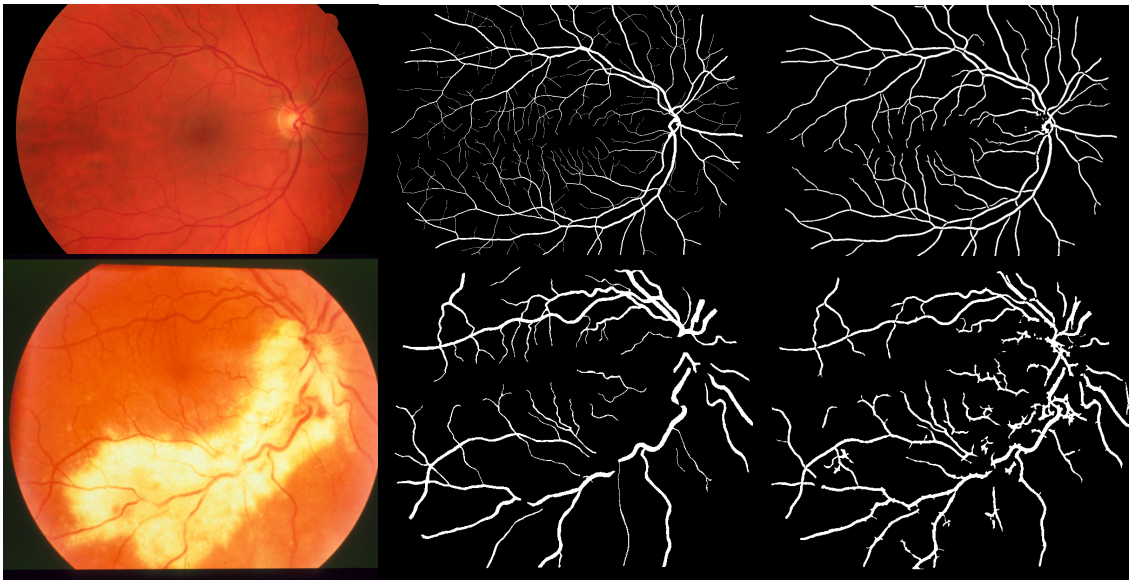

Figure 4: *Vessels segmentation examples.The first column represents the original images, in the middle the groundtruth, and the last column results of the proposed method.*

[KH16] KOVÁCS G., HAJDU A.: A self-calibrating approach for the segmentation of retinal vessels by template matching and contour reconstruction. *Med. Image Anal. 29* (2016), 24 – 46. 4

[LOD12] LEAHY C., O'BRIEN A., DAINTY C.: Illumination correction of retinal images using laplace interpolation. *Appl. Opt. 51*, 35 (Dec 2012), 8383–8389. 2

[LSAR17] L SRINIDHI C., APARNA P., RAJAN J.: Recent advancements in retinal vessel segmentation. *J Med Syst 41*, 4 (Mar 2017), 70. 1

[MAGAB11] MARIN D., AQUINO A., GEGUNDEZ-ARIAS M., BRAV J.: A new supervised method for blood vessel segmentation in retinal images by using gray-level and moment invariants-based features. *IEEE Trans. Med. 30* (2011), 146–158. 2

[MC06] MENDONÇA A., CAMPILHO A.: Segmentation of retinal blood vessels by combining the detection of centerlines and morphological reconstruction. *IEEE Trans. Med. 25*, 9 (2006), 1200–1213. 1, 3

[MLG*18] MERTEN N., LAWONN K., GENSECKE P., GROO., PREIM B.: Lung Vessel Enhancement in Low-Dose CT Scans - The LANCELOT Method. In *Bildverarbeitung für die Medizin (BVM)* (Erlangen, 2018), Springer Verlag, pp. 347–352. 3

[MMHM18] MOCCIA S., MOMI E. D., HADJI S. E., MATTOS L. S.: Blood vessel segmentation algorithms-review of methods, datasets and evaluation metrics. *Comput. Methods Programs Biomed. 158* (2018), 71 – 91. 1

[MPHT*07] MARTINEZ-PEREZ M., HUGHES A., THOM S., BHARATH A., PARKER K.: Segmentation of blood vessels from red-free and fluorescein retinal images. *Med. Image Anal. 11*, 1 (2007), 47–61. 2, 4

[OKB*13] ODSTRCILIK J., KOLAR R., BUDAI A., HORNEGGER J., JAN J., GAZAREK J., KUBENA T., CERNOSEK P., SVOBODA O., ANGELOPOULOU E.: Retinal vessel segmentation by improved matched filtering: evaluation on a new high-resolution fundus image database. *IET Image Proc. 7*, 4 (June 2013), 373–383. 1, 4

[OPB17] ORLANDO J. I., PROKOFYEVA E., BLASCHKO M. B.: A discriminatively trained fully connected conditional random field model for blood vessel segmentation in fundus images. *IEEE Trans. Biomed. Eng. 64*, 1 (Jan 2017), 16–27. 4

[PPP16] PANDA R., PUHAN N., PANDA G.: New binary hausdorff symmetry measure based seeded region growing for retinal vessel segmentation. *Biocybern Biomed Eng 36*, 1 (2016), 119 – 129. 1, 4

[SCBP14] SOARES I., CASTELO-BRANCO M., PINHEIRO A.: Microaneurysms detection using a novel neighborhood analysis. In *Proceedings of the Ophthalmic Med. Image Anal. First International Workshop, OMIA 2014, Held in Conjunction with MICCAI 2014* (Sept 2014), pp. 65–72. 2, 3

[SCBP16] SOARES I., CASTELO-BRANCO M., PINHEIRO A. M. G.: Optic disc localization in retinal images based on cumulative sum fields. *IEEE J. Biomed. Health. Inf. 20*, 2 (March 2016), 574–585. 2

[STA] Stare project website clemsoa university, clemson,sc[online]. Available from: <http://cecas.clemson.edu/∼ahoover/stare/>, Last accessed on 2018/08/20. 1

[tH05] TER HAAR F.: Automatic localization of the optic disc in digital colour images of the human retina. *M.S. thesis, Utrecht University, Utrecht, The Netherlands* (2005). 2

[Wit83] WITKIN A.: Scale-space filtering. *IJCAI'83 2* (1983), 1019–1022. 2

[WMM09] WINDER R. J., MORROW P. J., MCRITCHIE E. A.: Algorithms for digital image processing in diabetic retinopathy. *Comp. Med. Imag. and Graph. 33*, 8 (2009), 608–622. 2

[XNS*11] XU X., NIEMEIJER M., SONG Q., SONKA M., GARVIN M., REINHARDT J., ABRAMOFF M.: Vessel boundary delineation on fundus images using graph-based approach. *IEEE Trans. Med. Imag* (2011), 1184–1191. 1

[YBA*12] YU H., BARRIGA E., AGURTO C., ECHEGARAY S., PATTICHIS M., BAUMAN W., SOLIZ P.: Fast localization and segmentation of optic disk in retinal images using directional matched filtering and level sets. *IEEE Trans. Inf. Technol. 16*, 4 (2012), 644–657. 4

[ZDB*16] ZHANG J., DASHTBOZORG B., BEKKERS E., PLUIM J. P. W., DUITS R., TER HAAR ROMENY B. M.: Robust retinal vessel segmentation via locally adaptive derivative frames in orientation scores. *IEEE Trans. Med. Imaging 35*, 12 (Dec 2016), 2631–2644. 4